

Repurposing ubiquitination for innovative antibody conjugation

Hebieshy, A.F. el

Citation

Hebieshy, A. F. el. (2025, October 16). *Repurposing ubiquitination for innovative antibody conjugation*. Retrieved from https://hdl.handle.net/1887/4273517

Version: Publisher's Version

Licence agreement concerning inclusion of doctoral

License: thesis in the Institutional Repository of the University

of Leiden

Downloaded from: https://hdl.handle.net/1887/4273517

Note: To cite this publication please use the final published version (if applicable).



Targeted dendritic cell vaccination through ubi-tag-based peptide delivery

3

This chapter is part of the publication:

A.F. Elhebieshy*, Z. Wijfjes*, et al. Site-directed multivalent conjugation of antibodies to ubiquitinated payloads. Accepted for publication: Nature Biomedical Engineering.



Targeted Dendritic Cell vaccination through ubi-tag-based peptide delivery

Angela F. el Hebieshy, Zacharias Wijfjes, Camille M. Le Gall, Felix L. Fennemann, Cami M. P. Talavera Ormeño, Bjorn R. van Doodewaerd, Gerbrand J. van der Heden van Noort, Paul W. H. I. Parren, Martijn Verdoes, Huib Ovaa, Ferenc A. Scheeren.

Abstract

Targeted dendritic cell (DC) vaccination enhances antigen uptake and presentation, leading to more robust T cell responses against specific pathogens or tumor cells. In this study, we explored ubi-tagging as a promising conjugation technique for DC-targeted antigen delivery and compared its efficacy with that of the established sortagging method. We engineered the NLDC-145 hybridoma using the CRISPR/HDR platform to produce anti-mDEC205 Fab fragments fused to either a donor Ubi-tag or a sortag motif. We proceeded to conjugate the Fab fragments to the ovalbumin antigenic peptide SIINFEKL (OVAp) using ubitagging or sortagging respectively. In vitro assessments revealed that the ubitagged conjugates induced significantly higher levels of T cell activation markers and cytokine secretion compared to their sortagged counterparts. Encouraged by these results, we further evaluated the in vivo efficacy of both conjugates. Mice treated with ubi-tagged conjugates displayed a strong OT-I cell proliferation response, whereas sortagged conjugates showed minimal proliferation induction at this concentration. Biodistribution studies indicated that the ubi-tagged conjugates were preferentially taken up by CD11c+ dendritic cells, suggesting that this enhanced uptake contributes to improved T cell activation. Overall, our findings demonstrate the feasibility of ubi-tagging for DC-targeted antigen delivery, highlighting its potential advantages over traditional methods and its promise for future therapeutic applications.

Introduction

Dendritic cell (DC)-based immunotherapy has emerged as a promising approach to harness the immune system's capacity to target and eliminate cancer cells.¹ DCs are professional antigen-presenting cells that play a central role in linking innate and adaptive immunity by capturing, processing, and presenting antigens to T cells.²,³ Through this interaction, DCs can initiate a potent anti-tumor immune response by presenting antigenic peptides on major histocompatibility complex (MHC) molecules to T cell receptors (TCRs) on both CD4+ helper and CD8+ cytotoxic T cells.⁴,⁵ Moreover they provide co-stimulatory signals which strengthen the TCR mediated signals. This recognition process triggers the differentiation and proliferation of T cells, leading to targeted destruction of tumor cells and the secretion of cytokines that amplify the immune response.⁶⁻⁹

Traditionally, DC-based vaccines are generated by isolating DCs from a patient's blood, loading them with tumor antigens ex vivo, and reinfusing them back into the patient to stimulate a tumor-specific T cell response. 10-12 Since antigen presentation is highly dependent on the patient's unique HLA molecules (both MHC-II), using autologous DCs ensures compatibility and avoids the risk of immune rejection or suboptimal activation. 12,13 However, this ex vivo cellular therapy method is labor-intensive, time-consuming, and difficult to standardize, making it challenging for widespread clinical application. 12 To overcome these limitations, in vivo strategies have been developed to directly target DCs within patients, bypassing the need for cell isolation and manipulation. These approaches include the use of nanoparticles, liposomes, mRNA, and synthetic peptides for antigen delivery. 1,14-16 Additionally, antibodies that specifically bind to DC surface receptors have shown great potential for enhancing targeted delivery and improving T cell activation. 17-21

Among DC-specific targets, the C-type lectin receptor DEC205 (CD205) is of particular interest for DC targeted therapies, due to its specific expression on murine myeloid DCs.²² Targeting DEC205 with antibodies facilitates receptor-mediated endocytosis and subsequent antigen presentation, making it an attractive target for DC-focused vaccination strategies.^{23,24} Furthermore, targeted DC vaccination has been shown to promote cross-presentation—a unique process where DCs can present extracellular antigens on MHC-I molecules, which are typically used for presenting intracellular antigens.^{22–24} This ability enables DCs to simultaneously activate both CD4+ helper T cells (via MHC-II presentation) and CD8+ cytotoxic T cells (via MHC-I presentation), leading to a stronger and more coordinated anti-tumor response.²⁴

For effective DC targeting, peptide antigens need to be stably and specifically conjugated to antibodies that bind to DC surface receptors. However, current antigenantibody conjugation methods, such as thiol-based strategies, often result in conjugates with inconsistent antigen-to-antibody ratios and reduced binding affinity due to non-specific attachment.²⁵ More sophisticated approaches, such as recombinant fusion expression or site-specific chemo-enzymatic ligation (e.g., sortagging), have been developed to address these issues.¹⁷ Although these techniques offer better conjugation efficiency and maintain antibody functionality, they require additional reagents and complex purification steps, which can lower yields and complicate production processes.

To address these limitations, we used the ubi-tagging technology for the development of antibody-peptide conjugates for DC targeted vaccination. We used the anti-DEC205 antibody-producing hybridoma cell line NLDC-145, and engineered it to secrete monovalent Fab fragments fused to a donor ubi-tag. This donor ubi-tag was then subsequently used for conjugation to a fully chemically synthesized acceptor-ubitag carrying the ovalbumin-derived antigenic peptide SIINFEKL (OVAp) at its C-terminus. For comparison, we also generated conjugates using the same OVAp peptide fused to the

sortag motif through its respective conjugation enzymes. This design ensures precise site-specific conjugation and maintains the antibody's binding affinity for DEC205. Furthermore, using monovalent Fab fragments minimizes non-specific uptake via Fc receptors and enhances tissue penetration.

In this study, we evaluated the effectiveness of ubi-tagged and sortagged conjugates in terms of their ability to activate T cells and in vivo biodistribution. Our findings demonstrated that the ubi-tagged conjugates significantly enhanced T cell activation markers and cytokine secretion compared to the sortagged versions. Biodistribution studies revealed that the ubi-tagged conjugates were more selectively taken up by CD11c+ DCs in the spleen, which express DEC205, while the sortagged conjugates, despite using the same anti-DEC205 Fab fragment, were more frequently taken up by CD11b+ cells (likely macrophages, which do not express DEC205) and other splenocytes. The anti-DEC205 Fab ubiquitin conjugates showed therefore high target specificity. This differential uptake may be explained by variations in the solubility and aggregation tendencies of the two conjugates, which could affect their distribution and cellular interactions in vivo.

We hypothesize that the enhanced solubility and stability of ubi-tagged conjugates contribute to their improved targeting efficiency and T cell activation. Given these advantages, our platform has the potential to support the development of personalized DC-targeted vaccines incorporating multiple patient-specific tumor neoantigens. Such vaccines could enhance therapeutic efficacy by addressing the diverse mutational landscape and heterogeneity of tumors, thus paving the way for improved cancer immunotherapy strategies.

Results

Ubi-tagging for DC-targeted antigen delivery induces T cell activation in vitro

We explored ubi-tagging as a conjugation technique for dendritic cell (DC)-targeted antigen delivery and compared it to the alternative state-of-the-art chemoenzymatic conjugation technique, sortagging^{26,27}. To compare ubi-tagged-based and sortagged-based DC-targeted antigen delivery, we modified the NLDC-145 hybridoma using the CRISPR/HDR platform to produce anti-mDEC205 Fab fragments either linked to a Ub(K48R)^{don}-tag (Fig. 1a)or containing the LPESGG sortag-motif (Fab-Srt)^{28,29}. We selected the well-studied model ovalbumin epitope SIINFEKL (OVA_p, OVA₂₅₇₋₂₆₄)^{17,30}, which was attached to the C-terminus of either ubiquitin (Ub^{acc}-OVA_p) or a triglycine motif, via solid-phase peptide synthesis, with or without the FR-motif (Fig. 1b). This dipeptide motif was reported to enhance proteasome dependent cross-presentation for antigens delivered using NLDC-145 mAb¹⁷. After conjugation and purification, the OVA_p conjugates (Fig. 2a and Supplementary Fig. S1) were tested for their ability to induce antigen cross-presentation by DCs, as measured by their ability to activate SIINFEKL-specific CD8⁺ OT-I T cells *in vitro* (Fig. 2b). We observed high levels of activation markers

CD25, 4-1BB and CD44 on OT-I cells, as well as secretion of the pro-inflammatory cytokines interferon γ (IFN γ) and interleukin-2 (IL-2) in the Fab-Ub $_2$ -OVA $_p$ conditions, irrespective of the presence of the FR-motif (Fig. 2c-e and Supplementary Fig. S2). For the sortagged conjugates, the FR-motif appears crucial for T cell activation, consistent with earlier work¹⁷. The observed expression levels of activation markers and cytokine secretion suggest a more potent T cell activation by the Fab-Ub $_2$ -OVA $_p$ conjugates compared to the Fab-Srt-OVA $_p$ conjugates *in vitro* irrespective of the FR-motif (Fig. 2c-e).

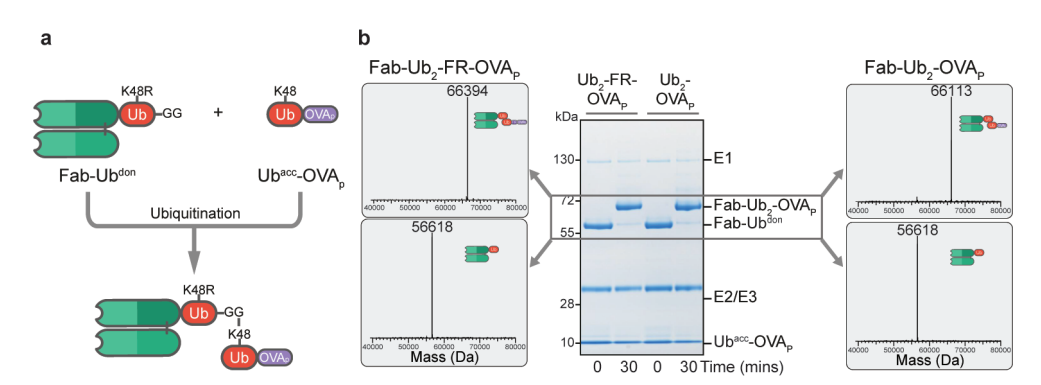


Figure 1 | **Ubi-tag conjugation of Fab-Ub**^{don} **to Ub**^{acc}-**OVA**_p (a) Schematic representation of ubi-tag conjugation of DEC205 Fab-Ub^{don} to chemically synthesized acceptor ubiquitin of which ovalbumin(257-264) peptide is attached to the C-terminus (Ub^{acc}-OVA_p). (b) Non-reducing SDS-PAGE analysis of the conjugation of Fab-Ub^{don} to either Ub^{acc}-FR-OVA_p or Ub^{acc}-OVA_p. The generated conjugates were isolated from the reaction mixture and the purity assessed using ESI-TOF mass spectrometry.

Ubi-tagged Fab-OVA $_{\rm p}$ conjugates targeting DCs result in potent T cell activation in vivo Encouraged by these results, we evaluated the ability of both Fab-Ub $_2$ -OVA $_{\rm p}$ and Fab-Srt-FR-OVA $_{\rm p}$ conjugates to induce OT-I activation *in vivo*. The day after adoptive transfer of CellTrace Violet (CTV)-labeled OT-I cells, mice were injected with a low dose (5 pmol, ± 12.5 ng/g + 10 µg LPS) of either conjugated anti-DEC205 Fab-Ub $_2$ -OVA $_{\rm p}$, Fab-Ub $_2$ -FR-OVA $_{\rm p}$, Fab-Srt-FR-OVA $_{\rm p}$, or a combination of unconjugated Fab-Ub(K48R)^{don} and Ub^{acc}-OVA $_{\rm p}$ or Ub^{acc}-FR-OVA $_{\rm p}$ (Fig. 2a). Two days after vaccination we evaluated the progressive dilution of CTV in the OT-I cells in the spleens and inguinal lymph nodes (Fig. 2b,c and Supplementary Fig. S3). We observed strong OT-I cell proliferation in the mice treated with the ubi-tagged conjugates, whereas the sortagged conjugate induced minimal OT-I proliferation at the dose used in this experiment. The ubi-tagged conjugates also induced stronger proliferation compared to the conditions in which unconjugated Fab-Ub and Ub-OVA $_{\rm p}$ s were given. This demonstrates the benefit of ubi-tagging of the targeting moiety, as well as the stability of the Fab-Ub $_{\rm p}$ conjugates *in vivo*.

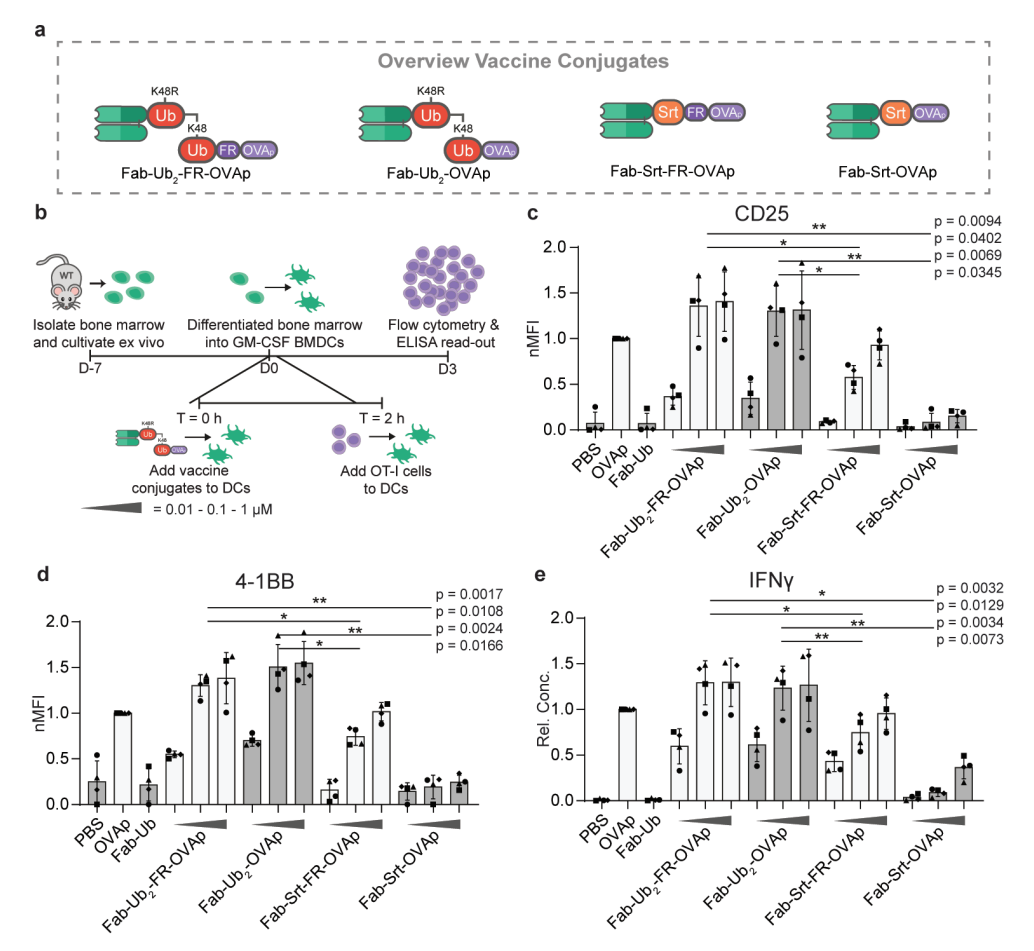


Figure 2 | Fab-Ub $_2$ -OVA $_p$ conjugates elicit potent T cell responses in vitro. (a) Schematic representation of anti-mDEC205 vaccine conjugates used in this experiment; Fab-Ub $_2$ -FR-OVA $_p$, Fab-Ub $_2$ -OVA $_p$, Fab-Ub $_2$ -

Biodistribution of ubi-tagged conjugates compared to sortagged conjugates

To gain insight into the observed differences in vaccine efficacy, we synthesized Fab-Ub $_2$ -K(DOTA-GA)-FR-OVA $_p$ and Fab-Srt-K(DOTA-GA)-FR-OVA $_p$ (Fig. 4a), which differ molecularly only in the linker type (ubi-tag vs sortag). Having these chelator-functionalized targeted vaccines in hand, we labeled them with radioactive 111 In and injected mice with the same

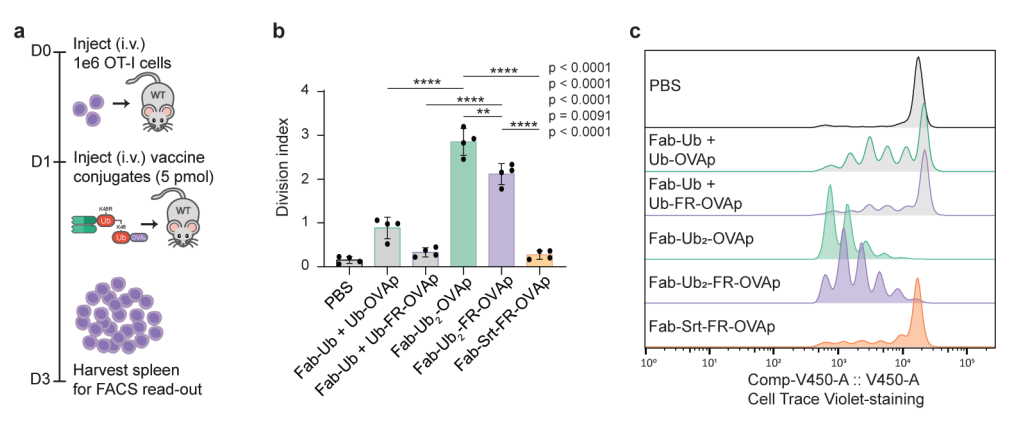


Figure 3 | Fab-Ub $_2$ -OVA $_p$ conjugates elicit potent T cell responses in vivo. (a) Schematic overview of in vivo OT-I cell activation assay. Mice (C57BL/6) received 1e6 CTV-labeled OT-I cells on day 0, followed by 5 pmol vaccine conjugate + 10 μ g LPS on day 1. Spleens were harvested on day 3. (b) Division index obtained by flow cytometry analysis (n = 4) of OT-I cells isolated from spleen. Data are shown as mean \pm SD. Unpaired T tests, p-values are noted in figure ****P<0.0001, **P<0.01. (c) Representative histograms of OT-I cell proliferation in spleen.

dose used for the vaccination experiments (5 pmol, ±12.5 ng/g vaccine + 10 µg LPS). Blood samples were taken over time until 24 hours post injection, at which point the biodistribution was determined. The blood clearance kinetics (Ub: fast t_{1/2}: 12.09 min., slow $t_{1/2}$: 139 min., Srt: fast $t_{1/2}$: 10.16 min, slow $t_{1/2}$: 88.79 min.) for the targeted vaccines are not significantly different (P=0.1179, F-test) (Fig. 4b and Supplementary Table S2a). A slightly higher concentration in the blood is observed at later time points for the ubitagged vaccine compared to the sortagged derivative, which we do not expected to be biologically relevant. The biodistribution data indicates that the ubi-tagged conjugate (molecular weight ~66 kDa) is primarily cleared via the liver and the sortagged conjugate (molecular weight ~52 kDa) through renal clearance (Fig. 4c and Supplementary Table S2b). This is in line with the molecular weight cutoff for glomerular filtration of 30-50 kDa³⁵. The remaining biodistribution data is very similar, with the exception of the higher uptake of the sortagged conjugate observed in the inguinal lymph node. To assess differences in cellular uptake within the spleen, different cell populations where isolated from the splenocytes, followed by measurement of the radioactivity in these isolated populations (Fig. 4d and Supplementary Table S2c). Interestingly, although the conjugates are equipped with the same DEC205-targeting Fab fragment, the ubi-tagged conjugate was more specifically taken up by the CD11c+ "dendritic cell" population, compared to the sortagged conjugate. The latter was taken up by the CD11c /CD11b+ population to a significantly higher degree. These data demonstrate superior in vivo target cell engagement of the ubi-tagged DC targeted vaccines, which helps explain the difference between the two conjugates in their ability to induce antigen-specific CD8⁺ T cell activation in the spleen (Fig. 3).

These results, together with the *in vivo* functionality of the anti-DEC205 Fab-Ub $_2$ -OVA $_p$ conjugates, demonstrate the feasibility of ubi-tagging as conjugation technique for DC-targeted antigen delivery, highlight the potential of ubi-tagging compared to the current state-of-the-art and provide a positive outlook for the use of ubi-tagged conjugates for other *in vivo* therapeutic applications.

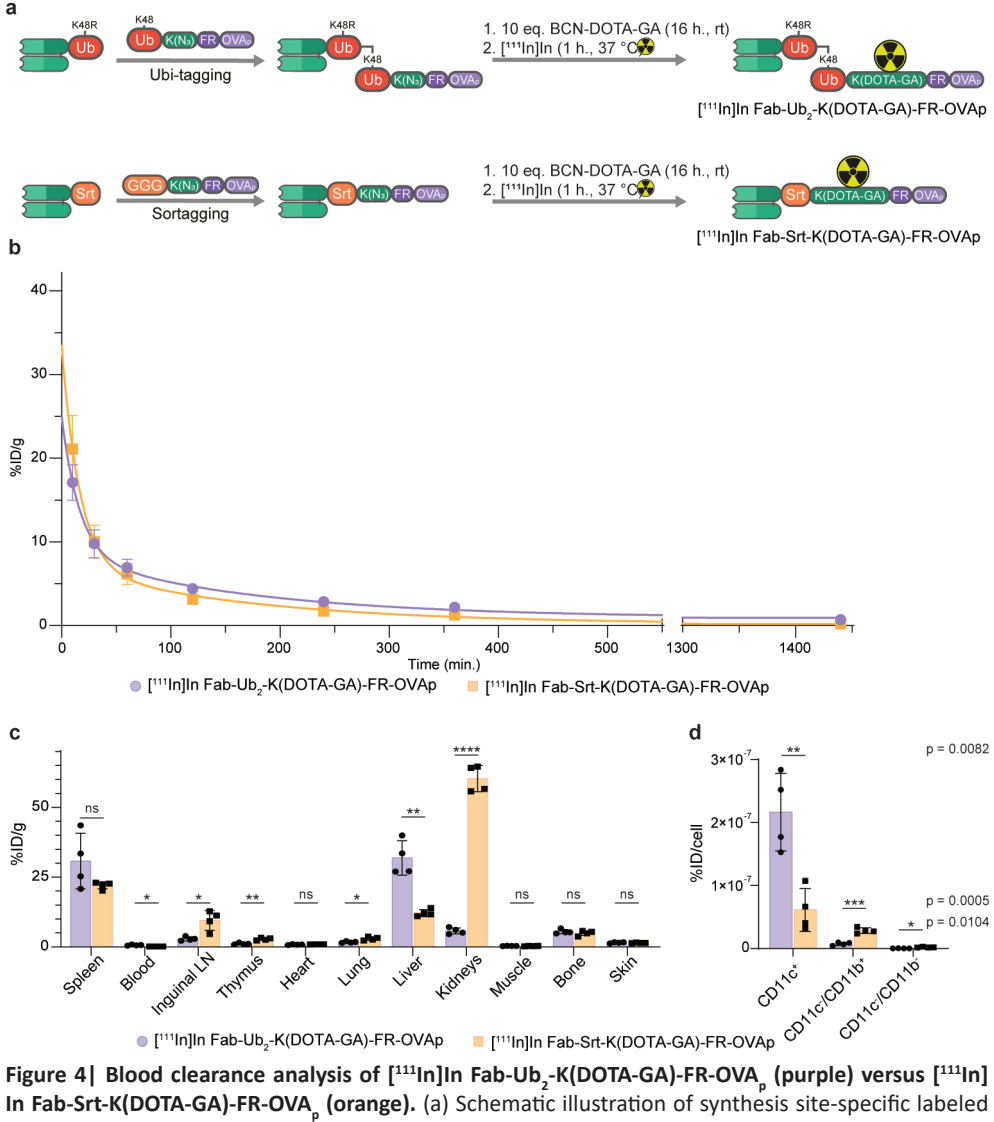


Figure 4| Blood clearance analysis of [111 In]In Fab-Ub $_2$ -K(DOTA-GA)-FR-OVA $_p$ (purple) versus [111 In] In Fab-Srt-K(DOTA-GA)-FR-OVA $_p$ (orange). (a) Schematic illustration of synthesis site-specific labeled DOTA-GA-conjugates. (b) Blood clearance analysis of [111 In]In Fab-Ub $_2$ -K(DOTA-GA)-FR-OVAp vs. [111 In] In Fab-Srt-K(DOTA-GA)-FR-OVAp. Data is depicted as mean percentage injected dose per gram (%ID/g) at several time-points with a two-phase decay curve fit (2 = 0.9640 for Ub-conjugate, 2 = 0.9507 for Srt-conjugate). F-testing indicates no significant differences between the two curve fits (2 = 0.1187). The calculated fast 1 _{1/2} for the Ub-conjugate is 12.09 min. and for the Srt-conjugate is 88.79 min. (c) Mice

(C57BL/6) were injected with 5 pmol 111 In-labeled Fab-Ub $_2$ -K(DOTA-GA)-FR-OVAp or Fab-Srt-K(DOTA-GA)-FR-OVAp + 10 µg LPS. Biodistribution was determined ex vivo 24 hours after injection (n = 4). Values are presented as percentage injected dose per gram (%ID/g). Data are shown as mean \pm SD. Unpaired T tests, p-values are noted in figure. ****P<0.0001, **P<0.001, *P<0.01, *P<0.05, ns P>0.05. (d) The spleens from (c) were dissociated and subsequently the CD11c $^+$ and CD11b $^+$ populations were isolated using MACS from the splenocytes, after which the radioactivity in all fractions was measured. Values are presented as percentage injected dose per cell (%ID/cell). Data are shown as mean \pm SD. Unpaired T tests, p-values are noted in figure. ***P<0.001, *P<0.01.

Discussion

In this work we explore the significance of ubi-tagging in the field of targeted antigen delivery. We also demonstrate the benefit of ubi-tag conjugation compared to the state-of-the-art ligation technique sortagging on potency to activate T cells in vitro and in vivo. Comparative blood clearance, biodistribution and in vivo target cell engagement data reveal that the ubi-tagged DC-targeted vaccines are more selectively taken up by DCs in the spleen, and show a higher on-target effect where they predominantly target DCs and not CD11b+ cells (presumably macrophages). However, the sortagged vaccine equipped with the same anti-DEC205 Fab fragment, was observed to be taken up by CD11b⁺ cells and other splenocytes showing a higher off-target effect. Differences in solubility and propensity to aggregation could be an explanation for this observation, but remains to be verified. The redundancy of the proteasomal cleavage FR-motif in these experiments hints towards different intracellular routing and processing, possibly by deubiquitinating enzymes. An alternative explanation could be that proteasome targeting is induced by the K48-linked di-ubiquitin. K48 tetra-ubiquitination is a well-known signal for proteasomal degradation. Yet, shorter ubiquitination-motifs also signal for proteasomal degradation^{31,32}. Follow-up studies will focus on further elucidation of the observed benefit in efficacy of ubi-tagged conjugates and will expand the use of ubi-tagging for targeted antigen delivery.

In summary, ubi-tagging provides a fast, efficient, and modular technique to generate well-characterized antibody conjugates of a wide variety of formats and combinations. Furthermore, significant improvements in T cell activation are observed when utilizing ubi-tagging as platform for antigen delivery compared to current state-of-the-art conjugation techniques. We expect the widespread adoption of this conjugation technique and its contribution to improving and developing protein conjugates, in particular antibody conjugates for preclinical research, diagnostic, and therapeutic applications.

Methods

General cell culture conditions

The hybridoma cell line NLDC-145 (ATCC HB-290) was modified for the stable expression of ubi-tagged antibodies or antibody fragments. Other cell lines used in this study were

EL4 (kindly provided by dr. Jacques Neefjes (LUMC, The Netherlands). The cell line NLDC-145 was cultured in Iscove's modified Dulbecco's medium (IMDM) (Gibco) supplemented with 7.5% fetal calf serum (FCS, Greiner). The cells were maintained at 37 °C and 5% CO₂, routinely examined by morphology analysis and tested for mycoplasma.

Cloning of CRISPR-Cas9 and donor constructs

The genomic sequence of the rlgG2a heavy chain locus was identified via the Ensembl rate genome build Rnor_6.0 and used for the design of the different HDR donor templates. gRNA for the rlgG2a constructs were previously described; for Hinge HDR constructs, gRNA-H, GACTTACCTGTACATCCACA, Addgene 124808; for isotype switch, gRNA-ISO (TGTAGACAGCCACAGACTTG, Addgene 124811) and ordered as single-stranded oligos from Integrated DNA Technologies (IDT) with the appropriate overhangs for cloning purposes. The oligos were phosphorylated with T4 PNK enzyme by incubation at 37 °C for 30 minutes and annealed by incubation at 95 °C for 5 minutes followed by gradually cooling to 25 °C using a thermocycler. The annealed oligos were cloned into the plasmid pSpCas9(BB)-2A-Puro (PX459), which was obtained as gifts from F. Zhang (Addgene plasmids 62988)³³. Synthetic gene fragments containing homologous arms and desired insert were obtained via Twistbioscience and cloned into the PCR4 TOPO TA vector (Thermo Fisher Scientific). All CRISPR-Cas9 and HDR constructs were purified with the NucleoBond Xtra Midi Kit (740410.100, Machery-Nagel) according to the manufacturer's protocol.

Hybridoma nucleofection with HDR and CRISPR-Cas9

Nucleofection of the HDR template and CRISPR-Cas9 vectors was performed with Cell Line Nucleofector Kit R (Lonza, VCA-11001) nucleofector 2b device. Before nucleofection hybridoma cells were assessed for viability and centrifuged (90g, 5 minutes), resuspended in PBS supplemented with 1% FBS and centrifuged again (90g, 5 minutes). 1x10⁶cells were resuspended in 100 μL Nucleofector medium with 1 μg of HDR template and 1 µg of CRISPR-Cas9 vectors or 2 µg of GFP vector (control) and transferred to cuvettes for nucleofection with the 2b Nucleofection System from Lonza (Program X001). Transfected cells were transferred to a 6-well plate in 4 mL of prewarmed complete medium. The following day the cells were transferred to a 10 cm petridish in 10 mL of complete medium, supplemented with 10-20 µg/mL of blasticidin (Invivogen, anti-bl-05). Antibiotic pressure was sustained until GFP-transfected hybridomas were dead and HDR transfections were confluent (typically between day 10-14). Cells were subsequently clonally expanded by seeding the hybridomas in 0.3 cells/well in round-bottom 96-well plates in 100 µL of complete medium. After onetwo weeks, supernatant from wells with a high cell density were obtained for further characterization and selected cloned were expanded.

Ubi-tag conjugation reaction

Ubi-tag conjugation reactions were carried out using 20 μM of aDEC205 Fab-Ub^{don} and 100 μ M of Ubacc-OVA in the presence of 0.25 μ M E1 enzyme, 20 μ M E2/E3 hybrid enzyme, 10 mM MgCl₂ and 5 mM ATP in PBS. For analysis of the reaction efficiency by SDS-PAGE, an initial reaction sample was taken from the reaction mixture prior to the addition of ATP. After the addition of ATP, the reaction was incubated at 37 °C for 30 minutes while shaking. Conjugation reaction samples were analyzed by quenching 2-5 μL of the reaction mixture in sample buffer and run in non-reducing conditions on 4-12% Bis-Tris gels (Invitrogen) by SDS-PAGE with MOPS as running buffer. Gels were stained using InstantBlue Coomassie Protein Stain (abcam) and imaged using Amersham600. Small-scale reactions were carried out on a scale corresponding to 2.5 µg ubi-tagged antibody fragments, while large-scale reactions were carried out on a 200 µg to 1 mg scale. Ubi-tagged Fab conjugates were purified from the reaction mixture by protein G affinity purification using a HiTrap Protein G HP column (GE Life Science) according to the manufacturer's protocol. The elution fractions containing purified conjugates were pooled, dialyzed against PBS, and concentrated using a 10 kDa Amicon Ultra centrifugal filter unit (Millipore). The purity of the ubi-tagged conjugates was assessed by SDS-PAGE and high-resolution mass spectrometry on a Waters Acquity H-class UPLC with XEVO-G2 XS Q-TOF mass spectrometer.

Solid-phase peptide synthesis

Solid-phase peptide synthesis (SPPS) of Rho-Ub was performed on a Syro II Multisyntech Automated Peptide synthesizer (SYRO robot; Part Nr: S002PS002; MultiSyntech GmbH, Germany) on a 25 μ mol scale using standard 9-fluorenylmethoxycarbonyl (Fmoc) based solid phase peptide chemistry. It was synthesized based on the procedure described by El Oualid *et al.*³⁴ using a fourfold excess of amino acids relative to pre-loaded Fmoc amino acid trityl resin (between 0.17 and 0.20 mmol/g, Rapp Polymere, Germany). All synthetic products were purified by RP-HPLC on a Waters preparative RP-HPLC system equipped with a Waters C18-Xbridge 5 μ m OBD (10 x 150 mm) column. The purified products were lyophilized and assayed for purity by high resolution mass spectrometry on a Waters Acquity H-class UPLC with XEVO-G2 XS Q-TOF mass spectrometer and by SDS-PAGE analysis.

Mass spectrometry

Mass spectrometry analysis was carried out on Waters ACQUITY UPLC-MS system equipped with a Waters ACQUITY Quaternary Solvent Manager (QSM), Waters ACQUITY FTN AutoSampler, Waters ACQUITY UPLC Protein BEH C4 Column (300 Å, $1.7 \mu m$, $2.1 \times 50 \text{ mm}$) and XEVO-G2 XS QTOF Mass Spectrometer (m/z = 200-2500) in ES+ mode.

Sample were run using 2 mobile phases: A = 1% MeCN, 0.1% formic acid in water and B = 1% water and 0.1% formic acid in MeCN with a runtime of 14 minutes. In the first 4 minutes, salts and buffer components were flushed from LC column using 98% A and 2% B. In the next 7.5 minutes, a gradient of 2-100% B was used, followed by 0.5 minutes of 100% B and subsequent reduction to 2% B and 98% A in 2 minutes. Data processing was performed using Waters MassLynx Mass Spectrometry Software 4.1, where the mass was obtained by deconvolution with the MaxEnt1 function.

Protein expression and purification

The E1 ubiquitin-activating enzyme UBE1 carrying an N-terminal His-tag was expressed from a pET3a vector in E. coli BL21(DE3) in autoinduction media for 2-3 hours at 37 °C, after which the bacteria were allowed to grow overnight at 18 °C. Next, bacteria were harvested and lysed by sonication, followed by His-affinity purification using Talon metal affinity resin (Clontech Inc., Palo Alto, CA, USA). Subsequently, the protein was further purified by anion exchange using a Resource Q column (GE Healthcare), followed by size exclusion using a Superdex 200 column (GE Healthcare).

The E2/E3 enzyme chimera plasmid was obtained as a gift from dr. Vincent Chau (Penn State, USA). The expression plasmid consists of the RING domain of the E3 ubiquitin ligating enzyme gp78 fused to the N-terminus of the E2 ubiquitin-conjugating enzyme Ube2g2 in a PET28a-TEV vector.

The E2/E3 enzyme chimera was expressed and purified as described 36 . In brief, the fusion protein was expressed in E. coli BL21(DE3) cells grown in LB at 37°C until OD $_{600}$ = 0.4-0.6 and induced with 0.4 mM IPTG for 4 hours at 30 °C. The harvested cells were lysed with Bugbuster protein extraction reagent (Millipore) according to manufacturer's protocol. The fusion protein was purified on Ni-NTA resin followed by size exclusion using a Superdex 200 column (GE Healthcare). Next, TEV protease cleavage was carried out overnight, and the cleaved fusion protein was further purified using a Resource Q column (GE Healthcare).

Ubi-tagged Fabs were produced in hybridoma cell lines engineered to produce Fabs fused at the C-terminus of the heavy chain to ubiquitin, followed by a His-tag at the C-terminus of ubiquitin. The modified hybridoma cells were cultivated for antibody production in CD Hybridoma medium supplemented with 2 mM ultraglutamine and 50 μ M β -mercaptoethanol for 7 to 10 days. To prevent the cleavage of the his-tag during cultivation, which is essential for blocking the C-terminal glycine residue of acceptor ubi-tags, antibodies fused to an acceptor ubi-tag were secreted in culture media supplemented with Ub-PA. However, donor ubi-tags require a free C-terminus; thus, antibodies fused a donor ubi-tag intended for conjugation were cultured without a DUB inhibitor. After 7 to 10 days, the culture media containing the ubi-tagged Fabs was centrifugated to remove cells. The supernatant was filtered through a 0.22 μ m

filter (GE Healthcare) and loaded on a pre-equilibrated HiTrap Protein G HP column (GE Life Science), and the ubi-tagged antibodies were purified according to the manufacturer's protocol. Elution fractions containing the ubi-tagged antibodies were pooled and dialyzed against PBS. Acceptor ubi-tagged antibodies, carrying a His-tag at the C-terminus of ubiquitin, were purified by Ni-NTA affinity purification prior to Protein G affinity purification (Supplementary Fig. 9).

Sortase-mediated chemoenzymatic ligation

aDEC205 Fab-Srt (1 eq., 20 nmol, 1 mg), 4s9 sortase (0.5 eq., 10 nmol, 0.18 mg) and GGG(FR)SIINFEKL (40 eq., 800 nmol, 0.91 mg) were added in sortase buffer (10% DMSO in 50 mM Tris HCl, 150 mM NaCl, 2 mM CaCl₂, pH = 7.5) and incubated (2 h., 37 °C). 100 μ L HisPurTM Ni-NTA Resin was added to the completed reaction and the mixture was incubated (15 min., rt) and centrifuged (10,000 rcf, 1 min., rt). The clear supernatant was purified by size exclusion chromatography (NGC, BioRad). The product was concentrated over a 10-kDa filter (Millipore). Concentration was determined using a NanoDropTM 2000 (ThermoFisher) and purity was assessed by SDS-PAGE (12%) analysis.

Site-specific generation DOTA-GA conjugates

Fab-Ub₂-K(N₃)-FR-OT-I (5 nmol, 0.33 mg) and Fab-Srt-K(N₃)-FR-OT-I (5 nmol, 0.25 mg) were conjugated as described above using ubi-tagging or sortase-mediated chemoenzymatic ligation respectively. After ligation, buffer was exchanged to metal-free PBS using Zeba spin desalting columns (0.5 mL, 7 kDa MW cut-off, Pierce Biotechnology). BCN-DOTA-GA (10 eq., 50 nmol, 14 μg) (C130, CheMatech) was added as 10 mM stock solution in DMSO and the final DMSO concentration was set at 10%. The reaction was incubated (16 h., rt) and purified using Zeba spin desalting columns (0.5 mL, 7 kDa MW cut-off, Pierce Biotechnology). Concentration was determined using a NanoDrop™ 2000 (ThermoFisher) and purity was assessed by SDS-PAGE (12%) analysis.

Radiolabeling

Conjugates (10 µg) were labeled under metal-free conditions with In-111 (Curium) (0.5 MBq/µg) in MES buffer (0.5 M, pH 5.5, 2x volume of 111InCl $_3$ solution). The mixture was incubated at 37 °C for 60 min. after which EDTA (final conc. 5 mM) was added. Radiochemical yield (RCY) of [111 In]In-Srt and [111 In]In-Ub conjugates was determined by instant thin-layer chromatography (iTLC) using silica gel coated paper (Agilent Technologies) with 0.1 M NH $_4$ OAc containing 0.1 M EDTA as mobile phase. iTLC strips were imaged using phosphor-luminescent plates on a phosphor imager (Typhoon FLA 7000, GE Healthcare). Purification was performed for all conjugates using Zeba spin desalting columns (0.5 mL, 7 kDa MW cut-off, Pierce Biotechnology). Purification was repeated once to obtain a radiochemical purity of >90%. Purified conjugates were

diluted in PBS for injection.

Mice

All mice were purchased from Charles River Laboratories, France. Female C57BL/6 WT and OT-I (Tg(TcraTcrb)1100Mjb/Crl) between 8-12 weeks of age and 18-25 g body weight were used for *in vitro* and *in vivo* experiments. Mice were sacrificed by cervical dislocation.

In vitro OT-I cell activation assay

BMDCs were generated as described below and plated at 10,000 cells per condition. Vaccine conjugates (1000 nM, 100 nM, 10 nM) were added to the BMDCs in 1:1 ratio of complete medium and PBS supplemented with LPS (0.3 μg/mL final concentration), and the BMDCs were incubated (2 h., 37 °C). In tandem, OT-I CD8+ cells were isolated as described below. After incubation with the vaccine conjugates, the BMDCs were washed and 50,000 OT-I cells were added to each condition. The BMDCs-OT-I cell coculture was incubated (3 d., 37 °C). The cells were spun down (1700 rpm., 2 min., 4 °C), supernatant was stored for ELISA analysis, and the cells were analyzed using a FACSVerseTM (BD Biosciences).

In vivo OT-I cell activation assays

OT-I CD8 $^{+}$ cells were isolated as described below and injected intravenously (1e6 cells, 100 μ L) into WT C57BL/6 mice (Charles River). After 24 h., the different vaccine conjugates (5 pmol) supplemented with LPS (10 μ g) in PBS were injected intravenously (100 μ L). 48 h. after injection of the vaccines, mice were cervical dislocated and the spleen and inguinal lymph nodes were harvested. Spleen cells were filtered and an ACK lysis was performed to remove red blood cells. Cells from the lymph nodes were filtered and pooled with the spleen cells to be analyzed using a FACSLyric (BD Biosciences).

GM-CSF BMDCs generation

Hindlegs of C57BL/6 (Charles River) were dissected. Tibia and femur were cleaned and cut open with a scalpel. Bone marrow cells were flushed out and collected in a petridish. 10 mL complete RPMI 1640 medium (ThermoFisher) supplemented with 50 μ M 2-mercaptoethanol and 25 ng/mL GM-CSF was added per 10e6 cells. On day 3, 5 mL fresh media (+ 50 μ M 2-mercaptoethanol, 25 ng/mL GM-CSF) was added. On day 8, non-adherent dendritic cells were harvested.

OT-I cell isolation

OT-I mice (C57BL/6-Tg(TcraTcrb)1100Mjb/Crl, Charles River) were killed by cervical dislocation and spleen and inguinal lymph nodes were harvested. Both organs were

meshed on a filter and splenocytes underwent ACK lysis. After lysis, splenocytes were pooled with lymphocytes and OT-I cells were isolated using magnetic-assisted cell sorting according to manufacturer's protocol (CD8α T Cell Isolation Kit, mouse, Miltenyi Biotec). Then, OT-I cells were stained with CellTrace™ Violet (ThermoFisher) for 20 min. at 37 °C and recovered in complete medium. Afterwards, cells were spun down (1500 rpm., 4 °C) and resuspended in PBS.

Blood kinetics and biodistribution

Mice (n = 4) were injected i.v. via the tail vein with [111 In]In-Srt conjugate or [111 In]In-Ub conjugate (5 pmol, ca. 0.1 MBq in 100 μ L PBS) pre-mixed with LPS (10 ug). Blood samples (ca. 20 μ L) were drawn via the vena saphena at various time points (10 min., 30 min., 1 h., 2 h., 4 h., 6 h.). 24 h. post injection, mice were euthanized via CO2 asphyxiation. Blood was obtained by cardiac puncture after which animals were dissected. Blood samples from various time points and isolated organs were weighed and counted in a gamma counter (Wizard 1480, PerkinElmer) along with standards to determine the % injected dose per gram (%ID/g) or % injected dose per organ (%ID). Stomach, small and large intestine were not emptied before y-counting.

Splenocyte subset isolation

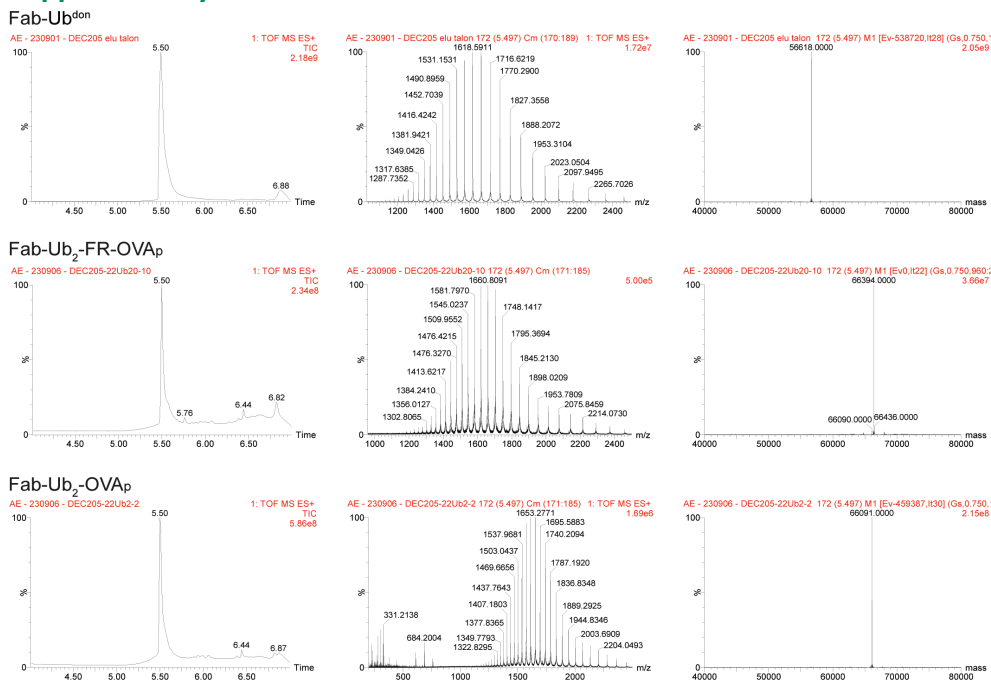
Spleens were recovered after y-counting and meshed on a filter. Splenocytes underwent ACK lysis and subsequently CD11c⁺ cells were isolated according to manufacturer's protocol (CD11c MicroBeads UltraPure, mouse, Miltenyi Biotec). In short, splenocytes were dissolved (4 μL buffer per 1e6 splenocytes) in MACS buffer (2 mM EDTA, 2% Fetal Bovine Serum in PBS) and CD11c⁺ magnetic beads (1 μL beads per 1e6 splenocytes) were added to the cells. The suspension was incubated at 4 °C for 10 min. and subsequently applied onto a pre-wetted LS column. The flowthrough and wash fractions containing CD11c splenocytes were collected and subjected to CD11b isolation according to the manufacturer's protocol (CD11b MicroBeads, human and mouse, Miltenyi Biotec). The CD11c⁺ splenocytes were eluted, counted using trypan blue, and γ-counted in a gamma counter (Wizard 1480, PerkinElmer). The CD11b+ isolation was performed equivalently to the CD11c⁺ isolation. The CD11c⁻/CD11b⁺ splenocytes were eluted, counted using trypan blue, and y-counted in a gamma counter (Wizard 1480, PerkinElmer). The flowthrough and wash fractions of CD11b⁺ isolation were collected and the CD11c⁻/ CD11b⁻ splenocytes were counted using trypan blue, and γ-counted in a gamma counter (Wizard 1480, PerkinElmer).

Flow cytometry and antibodies

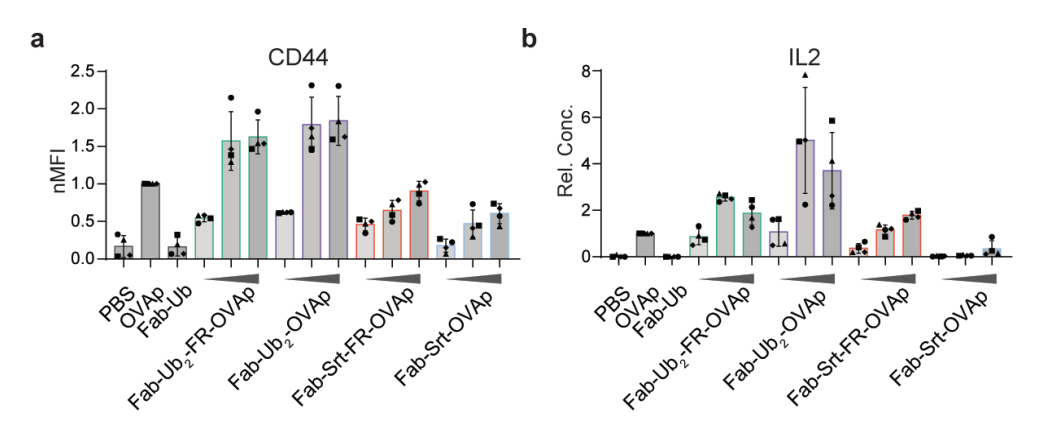
For FACS analysis, cells were washed with PBS, followed by life/death staining (20 min., rt) in 50 µL eBioscience™ Fixable Viability Dye eFluor™ 780 (1:2000, ThermoFisher).

Cells were washed once with PBA and antibody mixes were added (30 min., 4 °C). Cells were washed twice with PBA, taken up in 100 μL PBA and FACS analyses were performed on a FACSLyric[™] (BD Biosciences) or a FACSVerse[™] (BD Biosciences). The following antibodies were used for staining: mCD8α (1:100 dil., PerCP, clone 53-6.7, Biolegend), mCD8α (1:100 dil., FITC, clone 53-6.7, Biolegend), mCD25 (1:100 dil., FITC, clone PC61, Biolegend), mCD25 (1:100 dil., PerCP-Cy5.5, clone PC61, Biolegend), mCD44 (1:50 dil., PE/Cy7, clone IM7, Biolegend), m4-1BB (1:100 dil., APC, clone 17B5, ThermoFisher), mDEC205 (1:1000 dil., PE, clone NLDC-145, Biolegend), hCD8 (1:20 dil., APC, clone RPA-T8, BD Biosciences), hCD25 (1:50 dil., PE/Cy7, clone BC96, BioLegend), hCD69 (1:20 dil., PerCP, clone L78, BD Biosciences), h4-1BB (1:20 dil., PE, clone 4B4-1, BD Pharmingen).

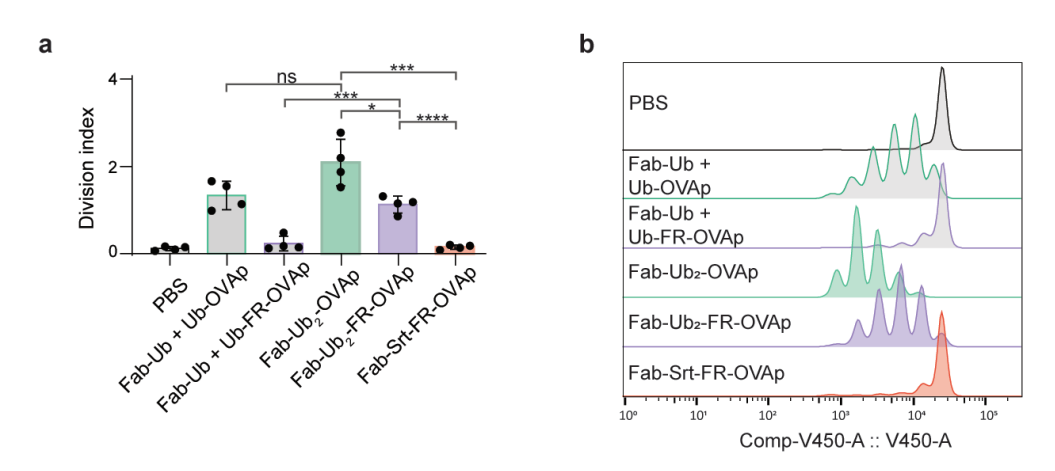
Supplementary information



S1 LC-MS analysis of α DEC205 Fab-Ub^{don} conjugation to either ub^{acc}-FR-OVA_p or Ub^{acc}-OVA_p forming Fab-Ub₂-FR-OVA_p or Fab-Ub₂-FR-OVA_p respectively. Total ion chromatograms (left), ESI-TOF spectra (middle) and deconvoluted ESI-TOF mass spectra (right).



S2 In vitro OT-I cell activation assay showing data for the T cell activation markers CD44 and IL2. GM-CSF BMDCs were generated and pulsed for 2 h. with 1000-100-10 nM vaccine conjugates or 1000 nM control conditions and 0.3 μ g/mL LPS. Sequentially, OT-I cells were added in 1:5 ratio and incubated for 3 days. Cells were analyzed using FACS. (c) FACS analysis. Statistics are provided in Table S1. Data (n = 4) are shown as mean \pm SD normalized MFI to positive control for CD44 (a) and IL2 (b).



S3 In vivo OT-I cell activation assay showing (a) flow cytometry analysis (n = 4) of division index of OT-I cells isolated from inguinal lymph nodes. Data are shown as mean ±SD. Paired T tests, ****P<0.0001, ***P<0.001, *P<0.005 (b) Representative histograms of OT-I cell proliferation in lymph nodes.

Table S1 Statistics for figure 2 and supplemental figure 2. All conditions are tested with a two-sided paired T test between conditions at similar concentrations. P values are notated in tables below, ****P<0.0001, ***P<0.001, **P<0.001, *P<0.005, ns P>0.05

Conditions compared		Figure 2C – CD25		
	At 1000 nM	At 100 nM	At 10 nM	
PBS vs Fab-Ub2-FR-OVAp	0.0083, **	0.0101, *	0.0055, **	
PBS vs Fab-Ub2-OVAp	0.0181, *	0.0075, **	0.0169, *	
PBS vs Fab-Srt-FR-OVAp	0.0027, **	0.0026, **	0.8161, ns	

PBS vs Fab-Srt-OVAp	0.2860, ns	0.5382, ns	0.6126, ns
Fab-Ub2-FR-OVAp vs Fab-Ub2-OVAp	0.1842, ns	0.1954, ns	0.7077, ns
Fab-Ub2-FR-OVAp vs Fab-Srt-FR-OVAp	0.1105, ns	0.0402, *	0.0092, **
Fab-Ub2-FR-OVAp vs Fab-Srt-OVAp	0.0075, **	0.0094, **	0.0053, **
Fab-Ub2-OVAp vs Fab-Srt-FR-OVAp	0.2424, ns	0.0345, *	0.0619, ns
Fab-Ub2-OVAp vs Fab-Srt-OVAp	0.0182, *	0.0069, **	0.0336, *
Fab-Srt-FR-OVAp vs Fab-Srt-OVAp	0.0011, **	0.0016, *	0.0313, *

Conditions		Figure 2D – 4-1BB			
Conditions compared	At 1000 nM	At 100 nM	At 10 nM		
PBS vs Fab-Ub2-FR-OVAp	0.0174, *	0.0073, **	0.0534, ns		
PBS vs Fab-Ub2-OVAp	0.0051, **	0.0066, **	0.0197, *		
PBS vs Fab-Srt-FR-OVAp	0.0166, *	0.0158, *	0.05129, ns		
PBS vs Fab-Srt-OVAp	0.9699, ns	0.5262, ns	0.5406, ns		
Fab-Ub2-FR-OVAp vs Fab-Ub2-OVAp	0.1598, ns	0.0863, ns	0.0116, *		
Fab-Ub2-FR-OVAp vs Fab-Srt-FR-OVAp	0.0273, *	0.0108,*	0.0059, **		
Fab-Ub2-FR-OVAp vs Fab-Srt-OVAp	0.0057, **	0.0017, **	0.0071, **		
Fab-Ub2-OVAp vs Fab-Srt-FR-OVAp	0.0098, **	0.0166, *	0.0071, **		
Fab-Ub2-OVAp vs Fab-Srt-OVAp	0.0024, **	0.0024, **	0.0055, **		
Fab-Srt-FR-OVAp vs Fab-Srt-OVAp	0.0020, **	0.0010, **	0.7975, ns		

Conditions compared		Figure 2E - IFNγ		
Conditions compared	At 1000 nM	At 100 nM	At 10 nM	
PBS vs Fab-Ub2-FR-OVAp	0.0022, **	0.0016, **	0.0089, **	
PBS vs Fab-Ub2-OVAp	0.0076, **	0.0020, **	0.0075, **	
PBS vs Fab-Srt-FR-OVAp	0.0017, **	0.0046, **	0.0053, **	
PBS vs Fab-Srt-OVAp	0.0126, *	0.0574, ns	0.2808, ns	
Fab-Ub2-FR-OVAp vs Fab-Ub2-OVAp	0.6742, ns	0.2087, ns	0.6052, ns	
Fab-Ub2-FR-OVAp vs Fab-Srt-FR-OVAp	0.0318, *	0.0129, *	0.0748, ns	
Fab-Ub2-FR-OVAp vs Fab-Srt-OVAp	0.0120, *	0.0032, *	0.0100, **	
Fab-Ub2-OVAp vs Fab-Srt-FR-OVAp	0.1268, ns	0.0073, **	0.0361, *	
Fab-Ub2-OVAp vs Fab-Srt-OVAp	0.0318, *	0.0034, **	0.0086, *	
Fab-Srt-FR-OVAp vs Fab-Srt-OVAp	0.0088, **	0.0065, **	0.0045, **	

Conditions compared		Figure S2 – CD44			
	At 1000 nM	At 100 nM	At 10 nM		
PBS vs Fab-Ub2-FR-OVAp	0.0003, ***	0.0032, **	0.0247, *		
PBS vs Fab-Ub2-OVAp	0.0005, ***	0.0014, **	0.0078, **		
PBS vs Fab-Srt-FR-OVAp	0.0087, **	0.0262, *	0.0764, ns		
PBS vs Fab-Srt-OVAp	0.0450, *	0.0412, *	0.9162, ns		
Fab-Ub2-FR-OVAp vs Fab-Ub2-OVAp	0.0393, *	0.0339, *	0.0592, ns		

Fab-Ub2-FR-OVAp vs Fab-Srt-FR-OVAp	0.0235, *	0.0336, *	0.0464,*
Fab-Ub2-FR-OVAp vs Fab-Srt-OVAp	0.0060, *	0.0020, **	0.0100, *
Fab-Ub2-OVAp vs Fab-Srt-FR-OVAp	0.0227, *	0.0150, *	0.0337, *
Fab-Ub2-OVAp vs Fab-Srt-OVAp	0.0090, **	0.0014, **	0.0024, **
Fab-Srt-FR-OVAp vs Fab-Srt-OVAp	0.0543, ns	0.3228, ns	0.0192, *

Conditions compared	Figure S2 – IL-2		
Conditions compared	At 1000 nM	At 100 nM	At 10 nM
PBS vs Fab-Ub2-FR-OVAp	0.0061, **	<0.0001, ****	0.0165, *
PBS vs Fab-Ub2-OVAp	0.0206, *	0.0211, *	0.0479, *
PBS vs Fab-Srt-FR-OVAp	0.0002, ***	0.0011, **	0.0626, ns
PBS vs Fab-Srt-OVAp	0.1769, ns	0.0474, *	0.8970, ns
Fab-Ub2-FR-OVAp vs Fab-Ub2-OVAp	0.0837, ns	0.1053, ns	0.4949, ns
Fab-Ub2-FR-OVAp vs Fab-Srt-FR-OVAp	0.7317, ns	0.0016, **	0.0197, *
Fab-Ub2-FR-OVAp vs Fab-Srt-OVAp	0.0070, **	<0.0001, ****	0.0179,*
Fab-Ub2-OVAp vs Fab-Srt-FR-OVAp	0.0812, ns	0.0392, *	0.0516, ns
Fab-Ub2-OVAp vs Fab-Srt-OVAp	0.0351, *	0.0221, *	0.0462, *
Fab-Srt-FR-OVAp vs Fab-Srt-OVAp	0.0092, **	0.0016, **	0.0567, ns

Table S2a Blood clearance data. Mice were treated as described in figure 5. %ID/g are given for the blood clearance study as shown in .

Timepoint	[111In]In Fab-Ub2-K(DOTA-GA)-FR- OVAp	[111In]In Fab-Srt-K(DOTA-GA)-FR- OVAp
	%ID/g	%ID/g
10 min.	17.1±2.1	21.1±4.01
30 min.	9.79±1.69	10.0±1.99
60 min.	6.92±1.03	6.16±1.25
120 min.	4.40±0.59	3.14±0.46
240 min.	2.84±0.39	1.71±0.20
360 min.	2.19±0.51	1.28±0.20
1440 min.	0.70±0.18	0.20±0.01

Table S2b Biodistribution data. Mice were injected as described in figure 5. %ID/g are given for the organs of which the weight was determined or as %ID for the stomach, small intestine, large intestine. Weight was not determined for the latter, as the organs were not emptied.

Tissue	[111In]In Fab-Ub2-K(DOTA-GA)-FR- OVAp	[111In]In Fab-Srt-K(DOTA-GA)-FR- OVAp
	%ID/g	%ID/g
Spleen	30.8±10.0	22.1±1.3
Blood	0.698±0.182	0.200±0.014
Inguinal LN	2.92±0.72	9.51±3.51

Thymus	1.19±0.29	2.88±0.46
Heart	0.888±0.121	0.965±0.025
Lung	1.77±0.29	3.01±0.62
Liver	31.9±6.2	12.2±1.2
Kidneys	5.77±1.10	60.34±4.73
Muscle	0.375±0.025	0.343±0.059
Bone	5.55±0.79	4.96±0.88
Skin	1.57±0.18	1.48±0.11
	%ID (e-3)	%ID (e-3)
Stomach	2.58±0.72	6.49±3.14
Small intestine	11.7±1.0	14.5±2.5
Large intestine	9.31±6.19	20.4±8.43

Table S2c Distribution data for splenocyte subset isolation. Mice were treated as described in Figure 5. %ID, cell number and %ID/cell are given for the isolation of the various splenocyte subsets.

Splenocyte	cyte [111In]In Fab-Ub2-K(DOTA-GA)-FR-OVAp		[111In]In Fab-Srt-K(DOTA-GA)-FR-OVAp		A)-FR-OVAp	
subset	%ID (e-5)	# Cells (e6)	%ID/cell (e-9)	%ID (e-5)	# Cells (e6)	%ID/cell (e-9)
CD11c+	25.3±12.5	0.13±0.09	216±62	6.32±1.15	0.13±0.06	61.5±34.1
CD11c-/ CD11b+	5.15±2.44	0.66±0.19	7.51±2.5	22.7±2.77	0.81±0.11	28.4±4.41
CD11c-/ CD11b-	3.88±1.92	11.4±9.1	0.40±0.14	27.4±8.29	13.0±4.11	2.18±0.66

Table S3 Rat IgG2A ubi-tagged Fab: donor and acceptor. Design HDR-template used to obtain the anti-DEC205 Fab-Ub^{don} and anti-DEC205 Fab-Ub^{acc}.

PCR4 TOPO	sequence
5'HA	CCTGGAACTCTGGAGCCCTGTCCAGCGGTGTGCACACCTTCCCAGCTGTCCTG-CAGTCTGGACTCTACACTCTCACCAGCTCAGCACCTGTCACCAGCTCTGACCAGCTCAGCACCTGGTC-CAGCCAGGCCACCTGCAACCTAGCCCAGCCAGCACCAAGGTGGA-CAAGAAAATTGGTGAGAACAACCAGGGGATGAGGGCCACCAGGGAGGG
Linker - Ub ₁₋₇₆ -His _{10x} (acceptor)	TGCCAAGGGAATGCGGAGGCGGTGGATCTATGCAAATTTTCGTTAAGACTCT-GACAGGGAAGACTATTACACTGGAGGTTGAGCCATCAGATACGATTGAGAAT-GTCAAGGCAAAGATACAGATACAGAAAGAAGGCT-GATCTTCGCTGGGAAGCAACAAGGCT-GATCTTCGCTGGGAAGCAACTGGAAGATGGCCGAACACTGAGCGATTATAACATA-CAAAAGGAGTCTACACTGCATTTGGTTCTGCGCCTTCGAGGCGGCATCACCACCACCACCACCACCACCACCACCACCACCACC

Linker - Ub _{K48R} -His _{10x} (Donor)	TGCCAAGGGAATGCGGAGGCGGTGGATCTATGCAAATATTCGTAAAGACTCTGACC-GGGAAAACCATTACACTTGAAGTGGAGCCGTCAGACACGATTGAGAATGTTAAGGC-TAAGATTCAGGACAAGGAAGGAAGGAAGGTATCCCGCCAGACCAACAACGCCTGATCTTCGCCG-GACGACAATTGGAGGATGGTAGGACTTTGAGCGATTACAACATACAGAAAGAA
IRES Bsr polyA	CCGGTGAGCTCTCCCTCCCCCCCCTAACGTTACTGGCCGAAGCCGCTTG-GAATAAGGCCGGTGTGCGTTTGTCTATATGTTATTTTCCACCATATTGCC-GTCTTTTTGGCAATGTGAGGGCCCGGAAACCTGGCCCTGTCTTCTTGACGAG-CATTCCTAGGGGTCTTTCCCCCCCCAAAGGAATGCAAAGGTCTGTTTGAATGTCGTGAAGGAAG
3'НА	GGTAAGTCACTAGGACTATTACTCCAGCCCCAGATTCAAAAAATATCCTCAGAGGCCCATGTTAGAGGATGACACAGCTATTGACCTATTTCTACCTTTCTTCATCTTACAGGCCCCATGTTAGAGGATGACACAGCTATTGACCTATTCTCCCCCCAAAGACCAAAGATGTGCCCCCCACAGAGACCAAAGATGTGCCCCAGAATGACCCCAGAGTCCACACTTAGGCCCAGAATGACCTTAAGGTCAGCTGGTTTATAGATGACGTGGAAGTCCACACACCTCAGACTCAGACTCCAGCTCAGACTCCAGCTCAGCTCAGTCCAGTCCAGCTCAATGCCCAGTGAACTCCCATCGTGCACCGGGACTGGCTCAATGGCAAAGTCAACACGCTCAAACCCGAAAGTCAACAGGAGCATTCCCTGCCCCCATCGAGAAAAGCATCTCCAAACCCGGAAGGTGGGAGCAGCAGGGTGTGAGAAGCTTCAAATGACTGAGGTGGGAGCAGCAGGGTGTGTGGTGTAGAAGCTGCAGTAGAACCATTAACTAGACTTAAAGGGCGAATTCGCGGCCGCGCCGCCGCCGCCGCCGCCGCCGCCGCCGC

Table S4 Rat IgG2a SrtA(4s9)-tagged Fab Design HDR-template used to obtain the anti-DEC205 Fab-Srt.

PCR2.1 TOPO	sequence
5'HA rIgG2a	CCTGGAACTCTGGAGCCCTGTCCAGCGGTGTGCACACCTTCCCAGCTGTCCTG-CAGCTCTGGACTCTACACTCTCACCAGCTCAGCACCTGTACCCTGACCTCACCAGCTCAGCACCTGGACCCAGCACCTGGACCAGCCCAGCACCAAGGTGGA-CAAGAAAATTGGTGAGAGAACAACCAGGGGATGAGGGCTCACTAGAGGTGAGGATA-AGGCATTAGATTGCCTACACCAACCAGGGTGGGCAGACATCACCAGGGAGGG
Linker – Sortag – HIS tag	GGAGGCGGAGCCTGCCGGAATCCGGCGCCACCATCACCATCACCATTGA
IRES Bsr polyA	GGATCCCAATTGCTCGAGGCCCCTCTCCCCCCCCCCTAACGTTACTGCCCGAAGCCGCTTGGAATAAGGCCGGTTGTGCTTTGTCTATATGTTATTTTCACCCATATTGCCGTTTTTGGCAATAGGCCGGTTGTGCTTTGTCTATATGTTATTTTCACCCATATTGCCGTCTTTTTGGCAATGTGAGGGCCCGGAAACCTGGCCCTGTCTTCTTGACGAGGCTTCTTTGAAGAGAAACAAGTCTGAATGTCGAAGGAAG
3'HA rIgG2a	GGTAAGTCACTAGGACTATTACTCCAGCCCCAGATTCAAAAAATATCCTCAGAGGCCCATGTTAGAGGATGACACAGCTATTGACCTATTTCTACCTTTCTTCATCTTACAGGCTCAGAAGTATCATCTGTCTTCATCTTCATCTTACAGGCTCAGAAGTATCATCTGTCTTCATCTTCCCCCCAAAGACCAAAGATGGCTCACCATCACTCTGACTCCTAAGGTCACGTGTGTTGTGGTAGACATTAGCCAGAATGATCCCGAGAGTCCAGCTGGTTTATAGATGACGTGGAAGTCCACAGCTCAGACTCAGTCCAGTCCAGTAGACTCCAACAGCACTTTACGCTCAGTCAG

References

- 1. Lee, K. W., Yam, J. W. P. & Mao, X. Dendritic Cell Vaccines: A Shift from Conventional Approach to New Generations. *Cells* **12**, (2023).
- 2. Banchereau, J. & Steinman, R. M. Dendritic cells and the control of immunity. *Nature* **392**, 245–252 (1998).
- 3. Mastelic-Gavillet, B., Balint, K., Boudousquie, C., Gannon, P. O. & Kandalaft, L. E. Personalized Dendritic Cell Vaccines-Recent Breakthroughs and Encouraging Clinical Results. *Front Immunol* **10**, (2019).
- 4. Oliveira, M. M. S. *et al.* Increased cross-presentation by dendritic cells and enhanced anti-tumour therapy using the Arp2/3 inhibitor CK666. *Br J Cancer* **128**, 982–991 (2023).
- 5. Joffre, O. P., Segura, E., Savina, A. & Amigorena, S. Cross-presentation by dendritic cells. *Nat Rev Immunol* **12**, 557–569 (2012).
- 6. Kurts, C., Robinson, B. W. S. & Knolle, P. A. Cross-priming in health and disease. *Nat Rev Immunol* **10**, 403–414 (2010).
- 7. Cabeza-Cabrerizo, M., Cardoso, A., Minutti, C. M., Pereira Da Costa, M. & Reis E Sousa, C. Dendritic Cells Revisited. *Annu Rev Immunol* **39**, 131–166 (2021).
- 8. Kaech, S. M., Wherry, E. J. & Ahmed, R. Effector and memory T-cell differentiation: implications for vaccine development. *Nat Rev Immunol* **2**, 251–262 (2002).
- 9. Curtsinger, J. M. & Mescher, M. F. Inflammatory cytokines as a third signal for T cell activation. *Curr Opin Immunol* **22**, 333–340 (2010).
- 10. Gu, Y. zhuo, Zhao, X. & Song, X. rong. Ex vivo pulsed dendritic cell vaccination against cancer. *Acta Pharmacol Sin* **41**, 959–969 (2020).
- 11. Wimmers, F., Schreibelt, G., Sköld, A. E., Figdor, C. G. & De Vries, I. J. M. Paradigm Shift in Dendritic Cell-Based Immunotherapy: From in vitro Generated Monocyte-Derived DCs to Naturally Circulating DC Subsets. *Front Immunol* **5**, (2014).
- 12. Constantino, J., Gomes, C., Falcão, A., Cruz, M. T. & Neves, B. M. Antitumor dendritic cell-based vaccines: lessons from 20 years of clinical trials and future perspectives. *Transl Res* **168**, 74–95 (2016).
- 13. Aarntzen, E. H. J. G. *et al.* Vaccination with mRNA-electroporated dendritic cells induces robust tumor antigen-specific CD4+ and CD8+ T cells responses in stage III and IV melanoma patients. *Clin Cancer Res* **18**, 5460–5470 (2012).
- 14. Van Lint, S. *et al.* Intratumoral Delivery of TriMix mRNA Results in T-cell Activation by Cross-Presenting Dendritic Cells. *Cancer Immunol Res* **4**, 146–156 (2016).
- 15. Pitt, J. M. *et al.* Dendritic cell-derived exosomes for cancer therapy. *J Clin Invest* **126**, 1224–1232 (2016).
- 16. Chen, Q. *et al.* Photothermal therapy with immune-adjuvant nanoparticles together with checkpoint blockade for effective cancer immunotherapy. *Nat Commun* **7**, (2016).
- 17. Swee, L. K. et al. Sortase-mediated modification of aDEC205 affords optimization

- of antigen presentation and immunization against a set of viral epitopes. *Proc Natl Acad Sci U S A* **110**, 1428–1433 (2013).
- 18. Gardner, A., de Mingo Pulido, Á. & Ruffell, B. Dendritic Cells and Their Role in Immunotherapy. *Front Immunol* **11**, (2020).
- 19. Caminschi, I., Maraskovsky, E. & Heath, W. R. Targeting Dendritic Cells in vivo for Cancer Therapy. *Front Immunol* **3**, (2012).
- 20. Lahoud, M. H. *et al.* Targeting antigen to mouse dendritic cells via Clec9A induces potent CD4 T cell responses biased toward a follicular helper phenotype. *J Immunol* **187**, 842–850 (2011).
- 21. Bonifaz, L. *et al.* Efficient targeting of protein antigen to the dendritic cell receptor DEC-205 in the steady state leads to antigen presentation on major histocompatibility complex class I products and peripheral CD8+ T cell tolerance. *J Exp Med* **196**, 1627–1638 (2002).
- 22. Jiang, W. *et al.* The receptor DEC-205 expressed by dendritic cells and thymic epithelial cells is involved in antigen processing. *Nature* **375**, 151–155 (1995).
- 23. Lehmann, C. H. K. *et al.* Direct Delivery of Antigens to Dendritic Cells via Antibodies Specific for Endocytic Receptors as a Promising Strategy for Future Therapies. *Vaccines 2016, Vol. 4, Page 8* **4**, 8 (2016).
- 24. Bonifaz, L. C. *et al.* In Vivo Targeting of Antigens to Maturing Dendritic Cells via the DEC-205 Receptor Improves T Cell Vaccination. *J Exp Med* **199**, 815 (2004).
- 25. Semmrich, M. *et al.* Directed antigen targeting in vivo identifies a role for CD103+ dendritic cells in both tolerogenic and immunogenic T-cell responses. *Mucosal Immunol* **5**, 150–160 (2012).
- 26. Antos, J. M., Truttmann, M. C. & Ploegh, H. L. Recent advances in sortase-catalyzed ligation methodology. *Curr Opin Struct Biol* **38**, 111–118 (2016).
- 27. Popp, M. W., Antos, J. M., Grotenbreg, G. M., Spooner, E. & Ploegh, H. L. Sortagging: a versatile method for protein labeling. *Nature Chemical Biology 2007 3:11* **3**, 707–708 (2007).
- 28. van der Schoot, J. M. S. *et al.* Functional diversification of hybridoma-produced antibodies by CRISPR/HDR genomic engineering. *Sci Adv* **5**, eaaw1822 (2019).
- 29. Birkholz, K. *et al.* Targeting of DEC-205 on human dendritic cells results in efficient MHC class II-restricted antigen presentation. *Blood* **116**, 2277–2285 (2010).
- 30. Carbone, F. R., Sterry, S. J., Butler, J., Rodda, S. & Moore, M. W. T cell receptor alpha-chain pairing determines the specificity of residue 262 within the Kb-restricted, ovalbumin257-264 determinant. *Int Immunol* **4**, 861–867 (1992).
- 31. Saeki, Y. Ubiquitin recognition by the proteasome. *J Biochem* **161**, 113–124 (2017).
- 32. Carroll, E. C., Greene, E. R., Martin, A. & Marqusee, S. Site-specific ubiquitination affects protein energetics and proteasomal degradation. *Nat Chem Biol* **16**, 866–875 (2020).

- 33. Ran, F. A. *et al.* Genome engineering using the CRISPR-Cas9 system. *Nature Protocols 2013 8:11* **8**, 2281–2308 (2013).
- 34. el Oualid, F. *et al.* Chemical synthesis of ubiquitin, ubiquitin-based probes, and diubiquitin. *Angewandte Chemie International Edition* **49**, 10149–10153 (2010).
- 35. Geurink, P. P. *et al.* Development of Diubiquitin-Based FRET Probes To Quantify Ubiquitin Linkage Specificity of Deubiquitinating Enzymes. *ChemBioChem* **17**, 816–820 (2016).
- 36. Blythe, E. E., Olson, K. C., Chau, V. & Deshaies, R. J. Ubiquitin- A nd ATP-dependent unfoldase activity of P97/VCP•NPLOC4•UFD1L is enhanced by a mutation that causes multisystem proteinopathy. *Proc Natl Acad Sci U S A* **114**, E4380–E4388 (2017).